Influence of the Boreal Summer Intraseasonal Oscillation on Extreme Temperature Events in the Northern Hemisphere

Yifei DIAO[1], Tim LI[1,2*], and Pang-Chi HSU[1]

1 *Key Laboratory of Meteorological Disaster, Ministry of Education/Joint International Research Laboratory of Climate and Environmental Change/Collaborative Innovation Center on Forecast and Evaluation of Meteorological Disasters, Nanjing University of Information Science & Technology, Nanjing* 210044, *China*
2 *International Pacific Research Center and Department of Atmospheric Sciences, School of Ocean and Earth Science and Technology, University of Hawaii, Honolulu, HI* 96822, *USA*

ABSTRACT

The impact of the boreal summer intraseasonal oscillation (BSISO) on extreme hot and cool events was investigated, by analyzing the observed and reanalysis data for the period from 1983 to 2012. It is found that the frequency of the extreme events in middle and high latitudes is significantly modulated by the BSISO convection in the tropics, with a 3–9-day lag. During phases 1 and 2 when the BSISO positive rainfall anomaly is primarily located over a northwest–southeast oriented belt extending from India to Maritime Continent and a negative rainfall anomaly appears in western North Pacific, the frequency of extreme hot events is 40% more than the frequency of non-extreme hot events. Most noticeable increase appears in midlatitude North Pacific (north of 40°N) and higher-latitude polar region.

Two physical mechanisms are primarily responsible for the change of the extreme frequency. First, an upper-tropospheric Rossby wave train (due to the wave energy propagation) is generated in response to a negative heating anomaly over tropical western North Pacific in phases 1 and 2. This wave train consists of a strong high pressure anomaly center northeast of Japan, a weak low pressure anomaly center over Alaska, and a strong high pressure anomaly center over the western coast of United States. Easterly anomalies to the south of the two strong midlatitude high pressure centers weaken the climatological subtropical jet along 40°N, which is accompanied by anomalous subsidence and warming in North Pacific north of 40°N. Second, an enhanced monsoonal heating over South Asia and East Asia sets up a transverse monsoonal overturning circulation, with large-scale ascending (descending) anomalies over tropical Indian (Pacific) Ocean. Both the processes favor more frequent extreme hot events in higher-latitude Northern Hemisphere. An anomalous atmospheric general circulation model is used to confirm the tropical heating effect.

Key words: boreal summer intraseasonal oscillation, extreme hot events, extreme cool events, Rossby wave train, monsoonal circulation

---

1. Introduction

Most of the operational meteorological centers in the world currently issue short-range (approximately 5 days) weather forecasts and seasonal outlooks. There is a gap in forecast skill in the intermediate scale (Say, between 5 and 30 days). Thus, the World Meteorological Organization (WMO) recently called for seamless whether–climate prediction to fill in the gaps between short-range weather forecast and long-range seasonal prediction.

Due to the requirements of national economy development and the prevention and reduction of natural disasters, there is an urgent need for the operational meteorological centers to develop the 10–30-day extended-range weather forecast capability. Extended-range forecast is an extension of current short-range forecast. At the moment, due to the lack of objective forecast methods and tools to support the operational forecast, extended-range forecasts are still in an experimental stage (e.g., Sun et al., 2008; Zhu et al., 2015).

A major predictability source for extended-range forecast is the occurrence of atmosphere intraseasonal oscillations (ISOs). In recent years, extreme weather and climate events occurred more frequently in a global context and brought in a greater impact on social economy. For example, Europe experienced an extremely hot summer in 2003. South China had a persistent ice rain and snow hazard in January 2008. A persistent severe drought happened in southwestern China in 2009 and 2010. Sometimes multiple extreme events happened in the same time over different regions of the world. For instance, heat waves hit the Northern Hemisphere from June to August in 2010, while extreme cold temperature events appeared in the Southern Hemisphere. It has been shown that signals from the atmospheric ISOs can be used for extended-range forecast (Li, 2000), because such signals have a direct linkage to short-term climate anomalies and the occurrence of extreme weather events as well.

Atmosphere intraseasonal oscillation, sometimes called "30–60-day oscillation", was first discovered by Madden and Julian (1971, 1972) with the analysis of observational data in Canton Island and other regions in the tropics. Using a spectral analysis, they detected a statistically significant signal in the atmospheric zonal wind, with a 40–50-day period and a slow eastward propagation speed along the equator. Subsequent studies with modern satellite data confirmed the planetary scale, eastward-propagating characteristics of the Madden–Julian Oscillation (MJO) (e.g., Weickmann, 1983; Lau and Chan, 1986), and showed that the oscillation is more broadband than the original 40–50-day period identified by Madden and Julian (1971, 1972) and can span a range of 20–100 days (see Li and Hsu, 2017 for a review on this topic).

MJO exhibits a distinctive seasonal evolution characteristic. In boreal winter, MJO is dominated by eastward propagation along the equator, whereas during boreal summer the eastward propagating mode weakens substantially (Hendon and Salby, 1994), while the northward propagation prevails in the Indian summer monsoon region (Yasunari, 1979; Jiang et al, 2004) and the northwestward propagation prevails over western North

Pacific (WNP) (Murakami, 1980; Lau and Chan, 1986). The fundamental cause of the seasonal difference lies in the geographic location of the thermal equator associated with the seasonal mean state between winter and summer (Li, 2014).

Due to the distinctive propagation characteristics between winter and summer, ISO activity in northern summer is often referred to as the boreal summer intraseasonal oscillation (BSISO) (e.g., Kemball-Cook and Wang, 2001). While the Real-time Multi-variate MJO (RMM) index (Wheeler and Hendon, 2004) has been widely used in operational centers for real-time MJO detection, Lee et al. (2013) proposed BSISO indices specifically for boreal summer, to better describe the northward propagation of ISO convection over the tropical Indian Ocean/western North Pacific sector. The BSISO indices proposed by Lee et al. (2013) contain two physical modes, with BSISO1 describing the northeastward propagation of convection (primarily over tropical Indian Ocean) at the time cycle of 30–60 days and BSISO2 describing northwestward propagation (mainly over western Pacific) at the time cycle of 10–30 days. The two indices seem better than RMM in capturing the observed BSISO propagation characteristics (Matsueda and Takaya, 2015).

Previous studies indicated that the main activity centers of the BSISO are confined over Bay of Bengal, South China Sea, and western North Pacific (Li and Wang, 2005). The convective activity associated with the BSISO over western North Pacific is considered as a key factor that influences regional extreme climate and weather events over East Asia (Ren and Huang, 2002; Li, 2010). Hsu et al. (2017) examined the impact of the BSISO on heat wave (HW) frequency over the Asian monsoon region. Chen and Zhai (2017) showed that active BSISOs could induce synchronous extremes of precipitation and temperature in East Asian coastal regions. Chen et al. (2018) investigated the relationship between large-scale circulation anomalies associated with the BSISO over the western Pacific and the occurrence of long-lived extreme heat events in South China, and concluded that the 5–25-day oscillation contributed mostly to the triggering and termination of the extreme heat events, whereas the 30–90-day oscillation plays a vital role in the persistence of long-lived extreme hot events. Less effort is made in understanding the effect of the BSISO on extreme temperature events in midlatitude Pacific and higher latitudes. Therefore, in this study, we will focus on the extreme temperature events in these regions.

In this paper, we will investigate the relationship between the BSISO phase and Northern Hemispheric ex-

treme temperature events and the physical mechanism responsible for the observed relationship. The resting paper is organized as following. In Section 2, data, analysis method, and numerical model used for this study are described. In Section 3, we reveal the observed relationship between the BSISO and extreme events. In Section 4, large-scale circulation patterns associated with active and inactive BSISO phases are examined, and possible mechanisms through which the BSISO affects the heat wave frequency are discussed. In Section 5, an anomaly general circulation model is employed to understand the effect of tropical heating associated with the BSISO on global temperature and circulation. In Section 6, we summarize the major results.

2.   Data, method, and model

2.1   *Data*

The primary data used in this study include daily average outgoing longwave radiation (OLR) from NOAA

(Liebmann and Smith, 1996), the reanalysis data generated by NCEP and the reanalysis data generated by ECMWF. The spatial resolution of the data above is 2.5° longitude × 2.5° latitude. The analysis period for the current study spans 30 yr from 1 January 1983 to 31 December 2012. Observed OLR is used as proxy for deep convection in the tropics. The major meteorological fields used in the NCEP reanalysis include zonal and meridional velocity, vertical p-velocity, temperature, and geopotential height on standard pressure levels.

2.2   *BSISO phase decomposition*

Using the empirical orthogonal function (EOF) analysis method, Lee et al. (2013) showed that there are two dominant BSISO modes in the tropical Indian Ocean and western Pacific domain. To reveal anomalous circulation features associated with the BSISO, the BSISO evolution is decomposed into eight phases, following Lee et al. (2013). Figure 1 illustrates the horizontal pattern and temporal evolution characteristics of the intraseasonal
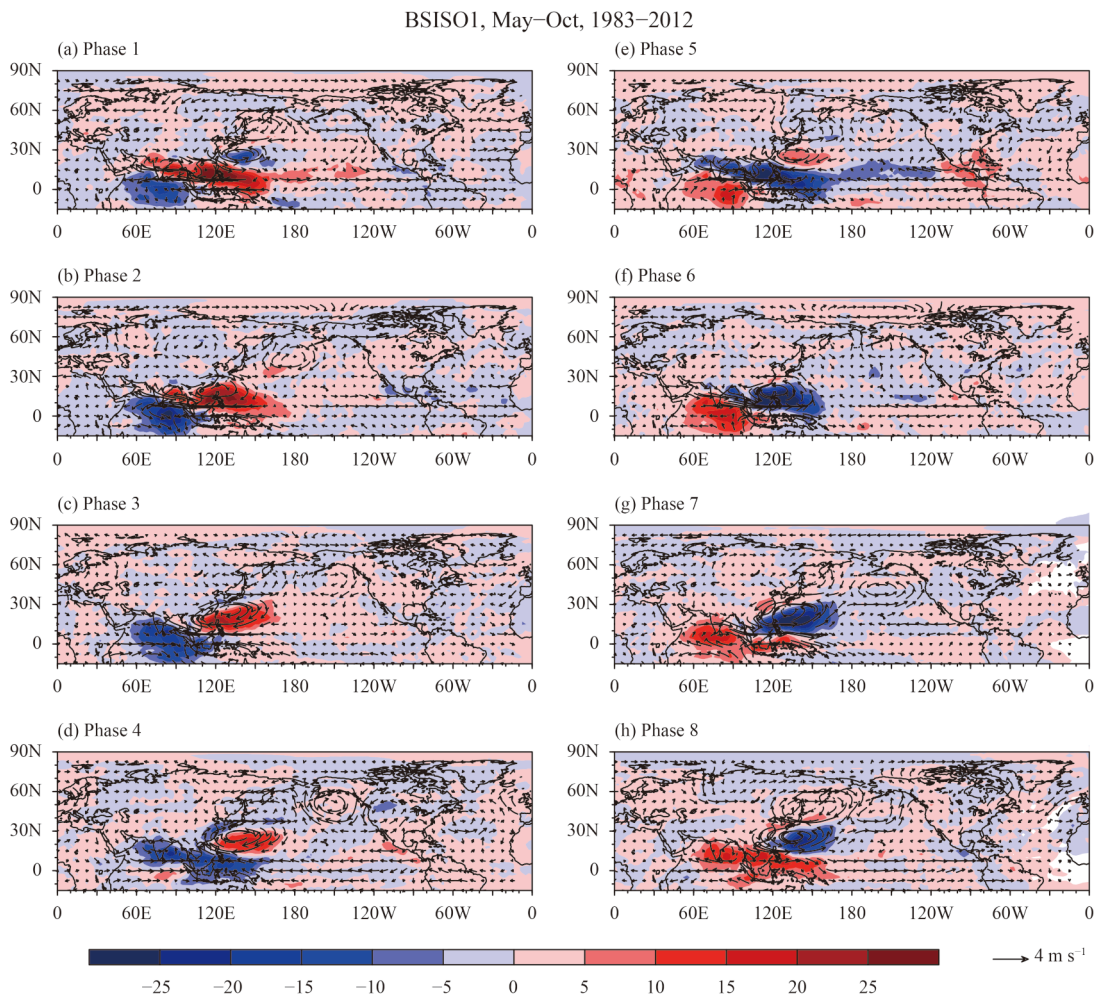

Fig. 1.   Composite OLR (shaded; W m^{-2}) and 850-hPa wind (vectors; m s^{-1}) anomalies during eight phases of BSISO1 from May to October.

OLR and 850-hPa wind fields associated with the first BSISO mode. At Phases 1 and 2, the major convection is located over the tropical Indian Ocean while a suppressed convective belt is oriented at a northwest–southeast direction, extended from Indian subcontinent to the Maritime Continent/western Pacific. At Phases 5 and 6, the OLR pattern is in general opposite to that in Phases 1 and 2. Accompanied to the enhanced (suppressed) convective belt is an anomalous cyclonic (anticyclonic) circulation pattern.

Figure 2 illustrates the OLR and wind evolution patterns for the second BSISO mode. Instead of northwest–southeast oriented rain band structure, the OLR field for BSISO2 shows a northeast–southwest tilted pattern. At Phases 1 and 2, enhanced convective rain-band appears in Philippine Sea and eastern equatorial Indian Ocean, while suppressed convection is observed over South China and South Japan. Given that the variance explained by BSISO2 is much smaller than BSISO1 and the period of the BSISO2 is more confined in the quasi-biweekly timescale, we will focus on examining

the response of global extreme temperature events to the first mode in the current study.

2.3 *Definition of extreme temperature events*

Daily mean temperature at 850 hPa is used to define extreme hot or cool events in northern summer from May to October, following Hsu et al. (2017). When daily mean temperature exceeds the 95th percentile, the date is defined as the extreme hot day. Similarly, when daily mean temperature is lower than the 5th percentile, the date is defined as the extreme cool day. The sum of the extreme hot and cool days during each phase of the BSISO during the 30-yr analysis period is then composed, to reveal how the extreme temperature events depend on the BSISO phase.

The definition above is done at each grid point so that the temperature thresholds differ spatially. Figure 3 shows the horizontal patterns for the extreme hot and cool temperature thresholds. Maximum and minimum values appear over high-latitude Asian and North American Continents along 60°N.
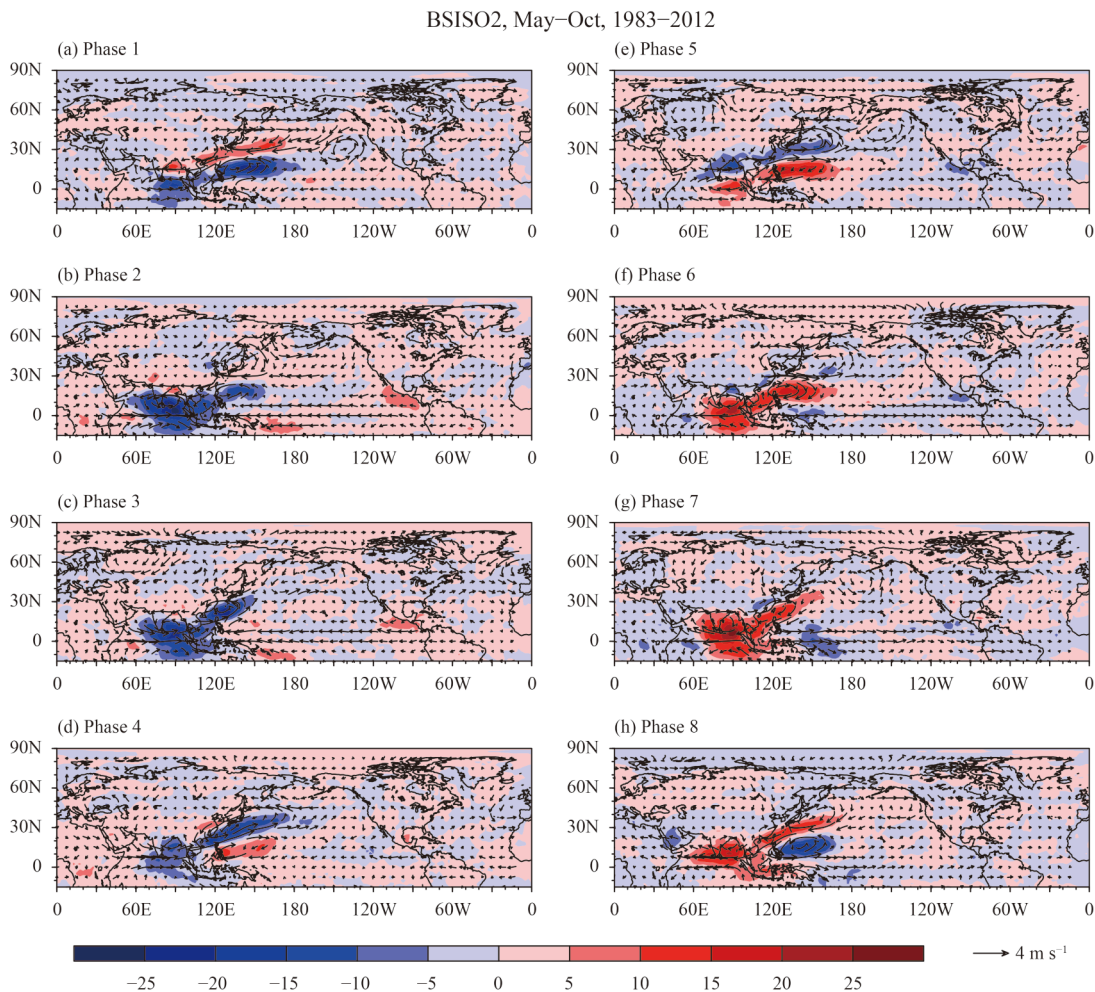

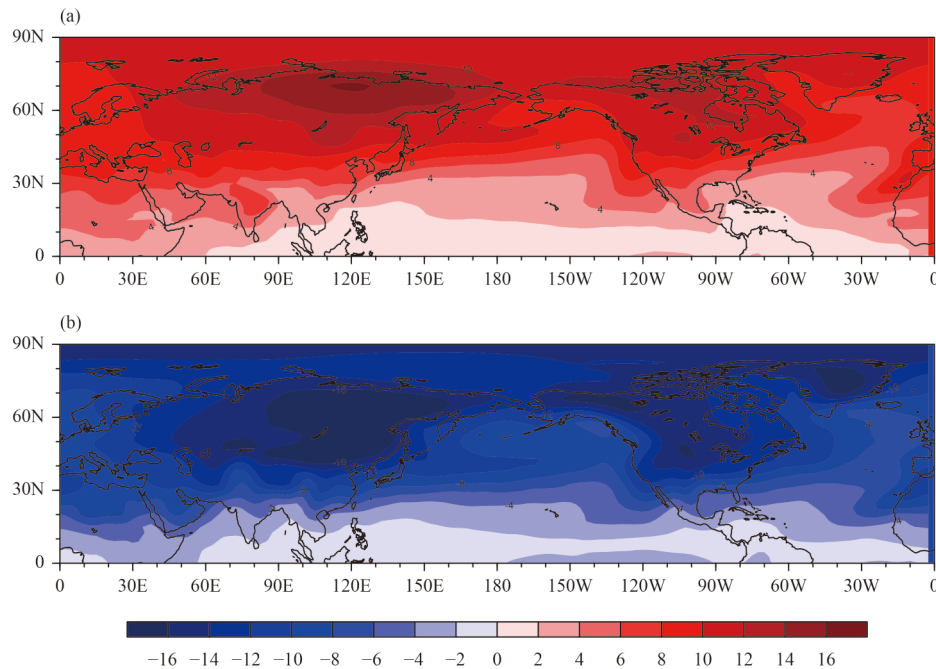Fig. 2. As in Fig. 1, but for the composite phases of BSISO2.

Fig. 3. 850-hPa temperature anomaly thresholds (K) for (a) extreme hot and (b) cool events averaged for the period from May to October.

2.4 *Monte Carlo statistical test*

A student *t*-test can be used for variables that have a normal (Gaussian) distribution. If a variable does not follow the normal distribution, then Monte Carlo test can be used. Monte Carlo technique is a statistical method used on the condition where it is difficult to find the answer by analytical methods. The method adopted here was developed by Ebisuzaki (1997), and was called random-phase test. Considering two time-series: A and B, which can be used to test the significance of correlation "*r*(A, B)" between A and B by following two steps. First, create *N* different random time series by analyzing the discrete Fourier analysis. All these time series will have the same power spectrum while different time phase compared to time series A. Second, *N* is set as 5000, following Wu et al. (2016).

In this study, A is the frequency of extreme temperature events during phases of BSISO1 with a 3–9-day lag, and B is the frequency of non-extreme temperature events during phases of BSISO1 with the same 3–9-day lag. We calculated the correlation between B and these random phase time series. If *r*(A, B) is equal or greater than 95% or equal or smaller than 5% compared with the random-phase time series, then it meets 10% significance level of statistical tests.

2.5 *An anomaly GCM*

An anomaly atmospheric model is employed to understand how the tropical heating anomaly associated with the BSISO may remotely affect the circulation and temperature fields in middle and high latitudes. This anomaly atmospheric GCM developed by Tim Li has been used in investigating how the summer (or winter) mean state modulates the monsoon response to El Niño induced equatorially symmetric heating (Wang et al., 2003), MJO initiation processes in western Indian Ocean (Jiang and Li, 2005), the instability of synoptic-scale wave train in the WNP (Li, 2006), and the Asia–North America teleconnection process (Zhu and Li, 2016).

The anomaly GCM was constructed based on the dry version of the Princeton AGCM (Held and Suarez, 1994). It is a global spectral model uses sigma as its vertical coordinate. The basic equations include momentum, temperature, and logarithm of surface pressure equations, together with the diagnostic equation for the vertical velocity. A specified 3D summer mean [June–August (JJA)] basic state is specified in the model so that one may examine how the atmosphere responds to a specific anomalous heating in the presence of the specified mean state. The model atmosphere is formulated with five evenly distributed sigma levels with an interval of 0.2, with sigma being zero at the top and one at the bottom. The horizontal resolution of the model is T42. Biharmonic diffusion is applied to the momentum and temperature equations with a dissipating rate of 0.1 day^{-1} for the smallest resolvable scale in the model. Rayleigh friction is applied to the momentum equations, with the damping rate of 1 day^{-1} in the lowest model level to mimic the

planetary boundary layer effect. Newtonian cooling with an e-folding time scale of 10 days is applied to the temperature equation at all levels. The model is integrated for 60 days, and the last 30-day average result is shown. For the detailed description of the model, readers are referred to the appendix in Jiang and Li (2005) and Li (2006).

3.　Dependence of extreme temperature events on BSISO phases

Previous studies (e.g., Matsueda and Takaya, 2015)

suggested that midlatitude circulation and temperature responses to tropical convection may lag by a few days, due to Rossby wave energy propagation. Hence, a 3–9-day lagged composite is conducted for all the analyses below. To test how the analysis result is sensitive to different lag times, we conducted a parallel calculation with 0–6- and 6–12-day lags, respectively, and found that the result is not sensitive. Due to low-frequency evolution characteristics, instead of illustrating eight phases, we only show combined four phases, with Phases 1–2, 3–4, 5–6, and 7–8. The upper panel of Fig. 4 shows the ratio of occurrence frequency of extreme hot events versus oc-
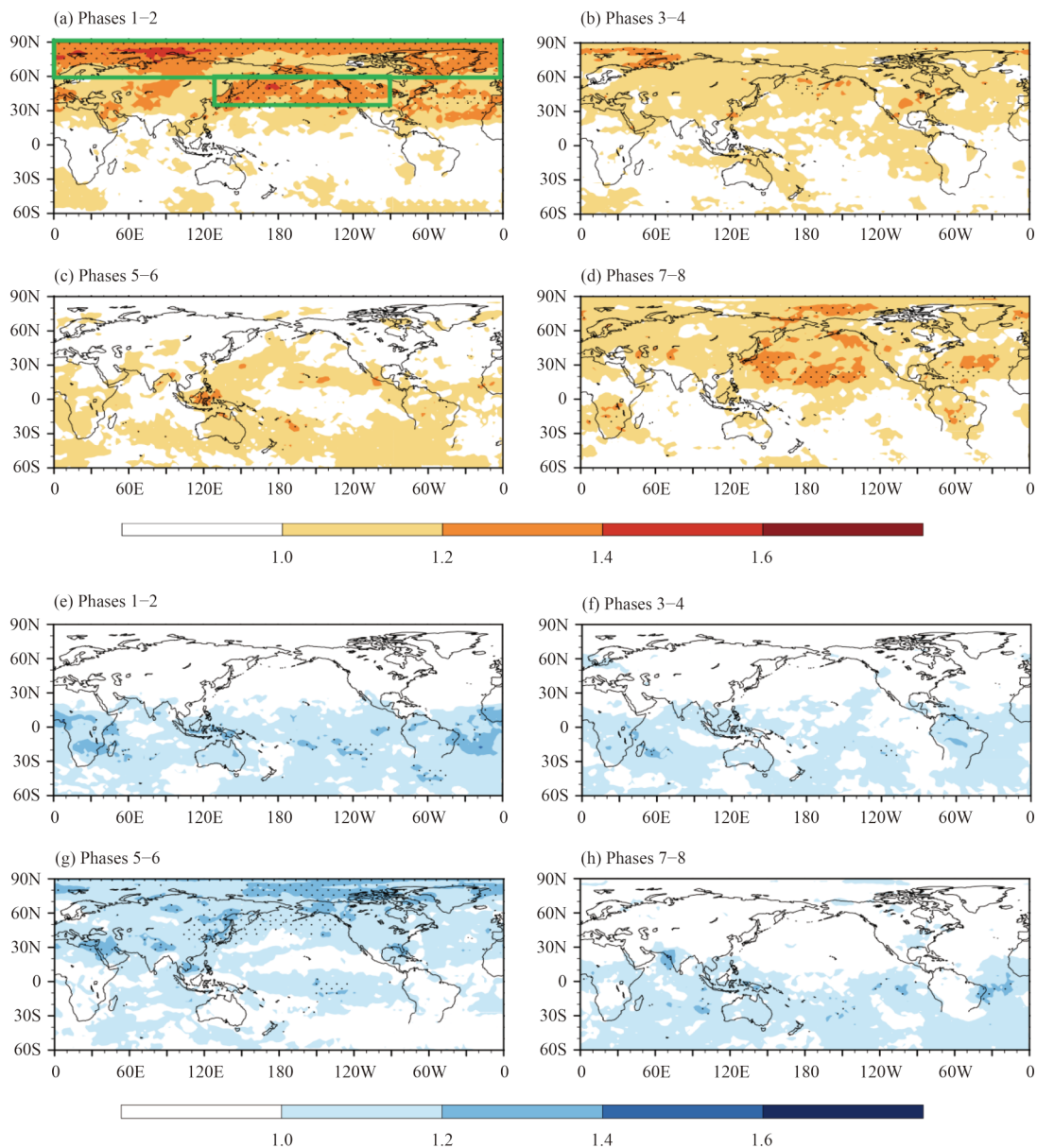

Fig. 4. Ratios of occurrence frequency (a–d) between extreme hot and non-extreme hot events, and (e–h) those between extreme cool and non-extreme cool events at 850 hPa during phases of BSISO1 with a 3–9-day lag. Black dots represent values reaching the 10% significance level with the Monte Carlo method.

currence frequency of non-extreme hot days during BSISO Phases 1–2, 3–4, 5–6, and 7–8, whereas the lower panel of Fig. 4 shows the ratio of occurrence frequency of extreme cool events versus occurrence frequency of non-extreme cool days during these BSISO phases. Only areas where the ratio exceeds one are shaded. It is clearly seen that extreme hot events in the Northern Hemisphere happened much more frequently during Phases 1–2 than during Phases 5–6. The extreme cool events, on the other hand, happened more frequently during Phases 5–6. Meanwhile, we do the same calculations based on the ERA-interim data, and obtained the consistent result.

The result indicates that the occurrence frequency of extreme hot or cool events in summer depends greatly on the phase of the BSISO. About 3–9 days after active BSISO convection appears over India and maritime continent, there are more frequent extreme hot events in the Northern Hemisphere, in particular, over midlatitude North Pacific (north of 40°N) and higher-latitude (beyond 60°N) polar regions. About 3–9 days after suppressed BSISO convection appears over India and maritime continent, there are less frequent extreme hot events but more frequent cool events in the Northern Hemisphere. The probability for occurrence of extreme hot events is about 40% more compared to that of occur-

rence of non-extreme hot days during BSISO Phases 1 and 2.

4. Atmospheric circulation anomalies associated with the BSISO phases

Because of the great contrast of the extreme event frequency between Phases 1–2 and Phases 5–6, hereafter we will focus on our analysis during these two phase periods. Figure 5 shows the precipitation and vertical p-velocity patterns during Phases 1–2 and 5–6. Consistent with the OLR patterns, enhanced rainfall occurs over the tropical Indian Ocean and Maritime Continent and suppressed precipitation appears over the WNP during Phases 1–2. Correspondingly, large-scale ascending motion anomalies occur in the tropical Indian Ocean, while large-scale descending motion anomalies appear over the large area of the Pacific. An approximately mirror image of the vertical motion anomalies appears during Phases 5–6.

The negative heating anomaly over the WNP may perturb the subtropical jet and trigger a Rossby wave train along a big circle (Hoskins and Karoly, 1981), which can be clearly seen in the geopotential height anomaly fields shown in Fig. 6. In the WNP heating region (near 20°N, 120°E), there is a clear baroclinic circulation response,
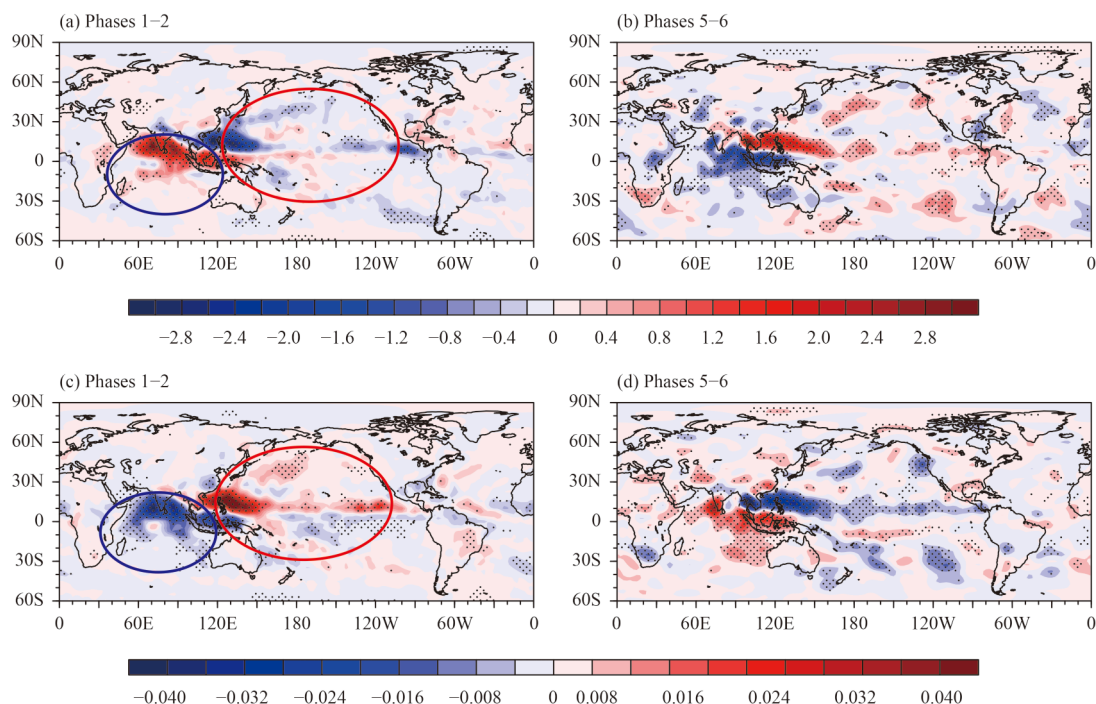

Fig. 5. (a, b) Composite precipitation anomaly (mm day^{-1}) and (c, d) composite 500-hPa omega anomaly (Pa s^{-1}) with a 3–9-day lag for BSISO1 (a, c) Phases 1–2 and (b, d) Phases 5–6. The red circle represents the overall large-scale descending motion or suppressed precipitation region and the blue circle represents the overall large-scale ascending motion or enhanced precipitation region. Black dots represent values exceeding the 90% confidence level (Student t-test).

with a low pressure anomaly in the upper level and a high pressure anomaly in the low level. To the northeast of the forcing region, a wave train is clearly seen in the 200-hPa field, with an alternative high–low–high pressure pattern, forming a big circle extending from North of Japan to the western coast of United States. Note that within the wave train, the two high pressure centers are much stronger than the low pressure center, which is located further to the north. The wave train in midlatitudes has a clear equivalent barotropic structure, different from the tropical system.

Due to the quasi-geostrophic nature, the wind anomaly field in midlatitudes is closely associated with the pressure field. In the upper troposphere, the most pronounced circulation feature along the wave train is the occurrence of two anomalous anticyclones (upper panel of Fig. 7), which are in phase with the two high pressure centers. The cyclonic circulation is weaker and located further to the north. As a result, the zonal mean wind near 40°N is dominated by easterly anomalies. The anomalous circulation patterns are quite similar throughout the troposphere (lower panels of Fig. 7), and their amplitude decreases towards the surface. According to the hydrostatic relation, an expansion of the air column is related to a warmer temperature between two constant pressure levels. Physically, one may argue that stronger anomalous anticyclone in the upper-level could induce anomalous descent motion below, which is favorable for more vertical adiabatic heating and more solar radiation into the surface, and thus leads to a higher temperature anomaly. As a result, the tropospheric warming anomalies appear north of the weakened climatological jet. An opposite pattern in the geopotential height, temperature and wind fields appears during Phases 5–6.

To show more clearly how the tropical heating induced wave train pattern affects the zonal mean wind, we plotted the meridional–vertical cross sections of zonal mean climatological and anomalous temperature and zonal wind fields, which are shown in Fig. 8. The climatologic summer mean subtropical jet is located near 40°N. It is interesting to note that the strength of the subtropical jet weakens during Phases 1–2 but strengthens
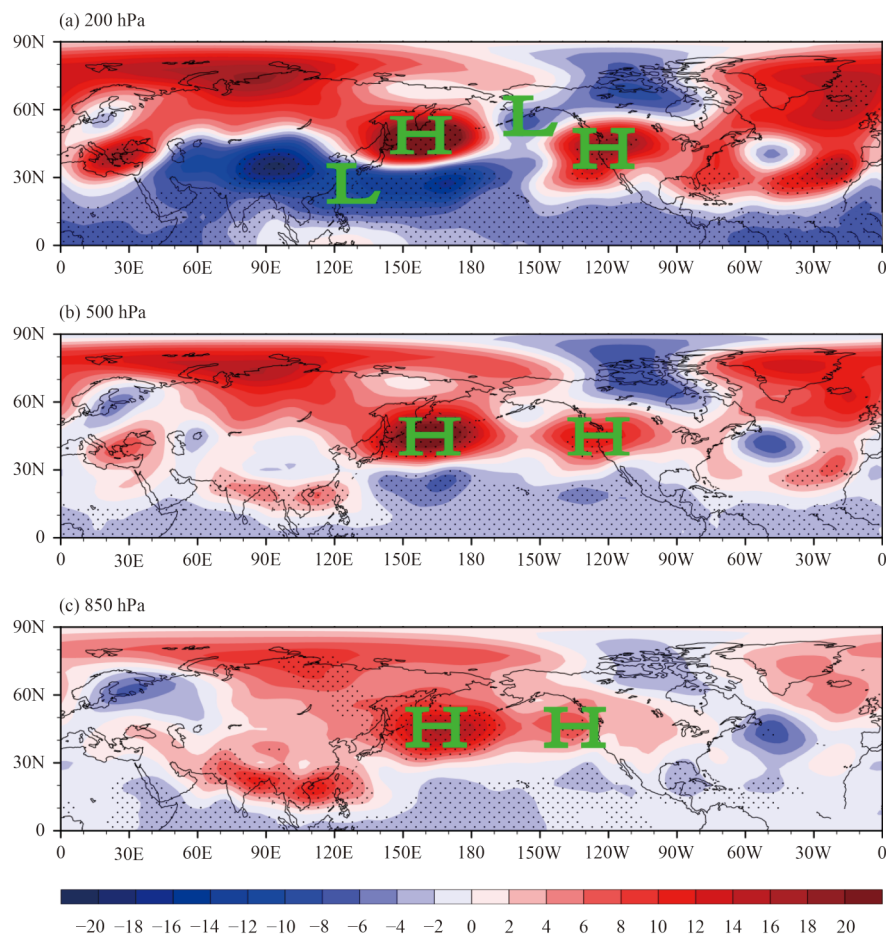

Fig. 6. Composite geopotential height anomaly fields (gpm) at (a) 200, (b) 500, and (c) 850 hPa with a 3–9-day lag for BSISO1 Phases 1–2. Black dots represent values exceeding the 95% confidence level (Student *t*-test).

Fig. 7. Composite vorticity (shaded; s^{-1}) and wind (vector; m s^{-1}) anomaly fields at (a) 200, (b) 500, and (c) 850 hPa with a 3–9-day lag for BSISO1 Phases 1–2. Black dots represent values exceeding the 95% confidence level (Student t-test).
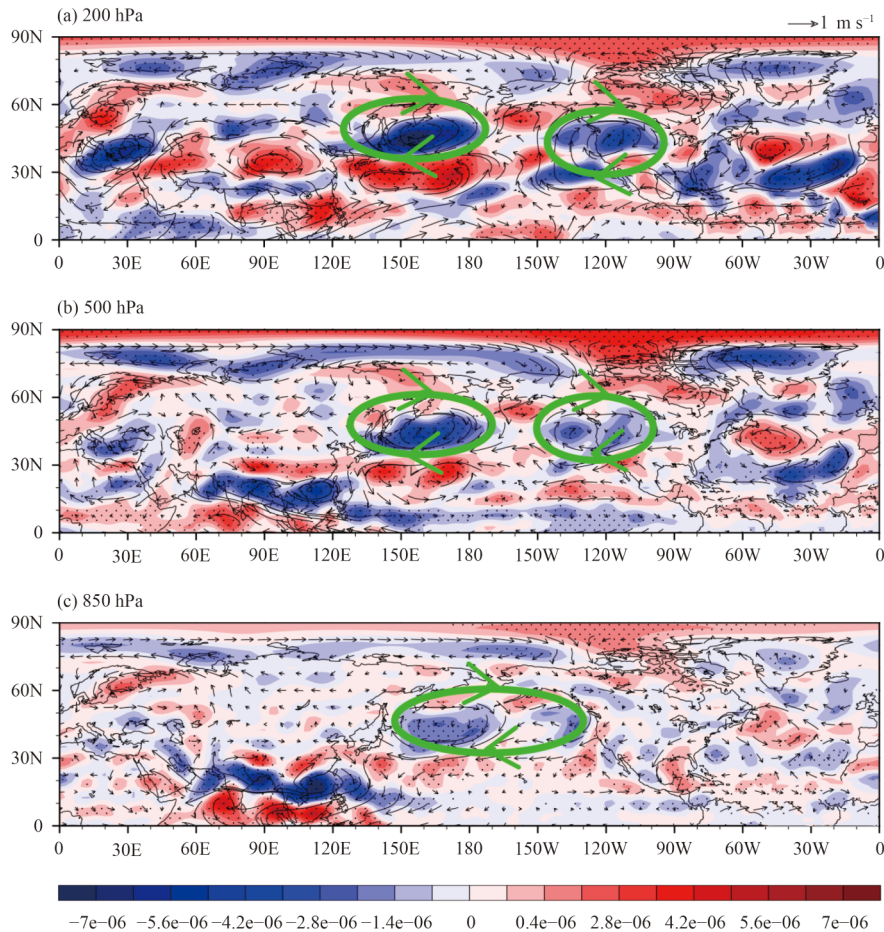
during Phases 5–6. According to the thermal wind balance, a weakened jet is associated with a weakened meridional temperature gradient, with a tropospheric warming (cooling) to the north (south) of the jet. Such a temperature change is clearly seen in Fig. 8b. An opposite pattern is seen during Phases 5–6.

The wave train induced zonal wind and temperature changes well explain why more frequent hot (cool) events appear north of 40°N during Phases 1–2 (Phases 5–6). To further explain the regional characteristic, for example, a maximum center over midlatitude North Pacific, one needs to further examine the horizontal distribution of the climatological subtropical jet and anomalous wind patterns. Figure 9a shows the horizontal map of climatological summer mean zonal wind field at 200 hPa. Note that the main subtropical jet axis is oriented in the southwest–northeast direction, with a maximum jet center at 140°E near Japan. The momentum equation in a Lagrangian framework may be written as:

$$\frac{du}{dt} = f(v - v_g) = f \cdot v_a, \qquad (1)$$

where v_g denotes the meridional component of geostrophic wind, and u and v denote actual zonal and meridional wind components, respectively. To the west (east) of the jet center, air parcel accelerates (decelerates) along the wind direction so that $\frac{du}{dt}$ is positive (negative). This excites the secondary circulation with ageostrophic meridional wind toward north (south) to the west (east) of the jet center. To the east of the jet center, the southward ageostrophic wind further causes an upper-level convergence (divergence) to the south (north), leading to descending (ascending) motion in middle troposphere.

During Phases 1–2, strong easterly anomalies occur near the climatological jet center. This weakens the jet intensity, promoting anomalous northward ageostrophic wind to the east of the jet center. Consequently, upper-level convergence anomalies appear in the north of the jet stream while low-level divergence anomalies appear in the south of the jet stream. This causes anomalous
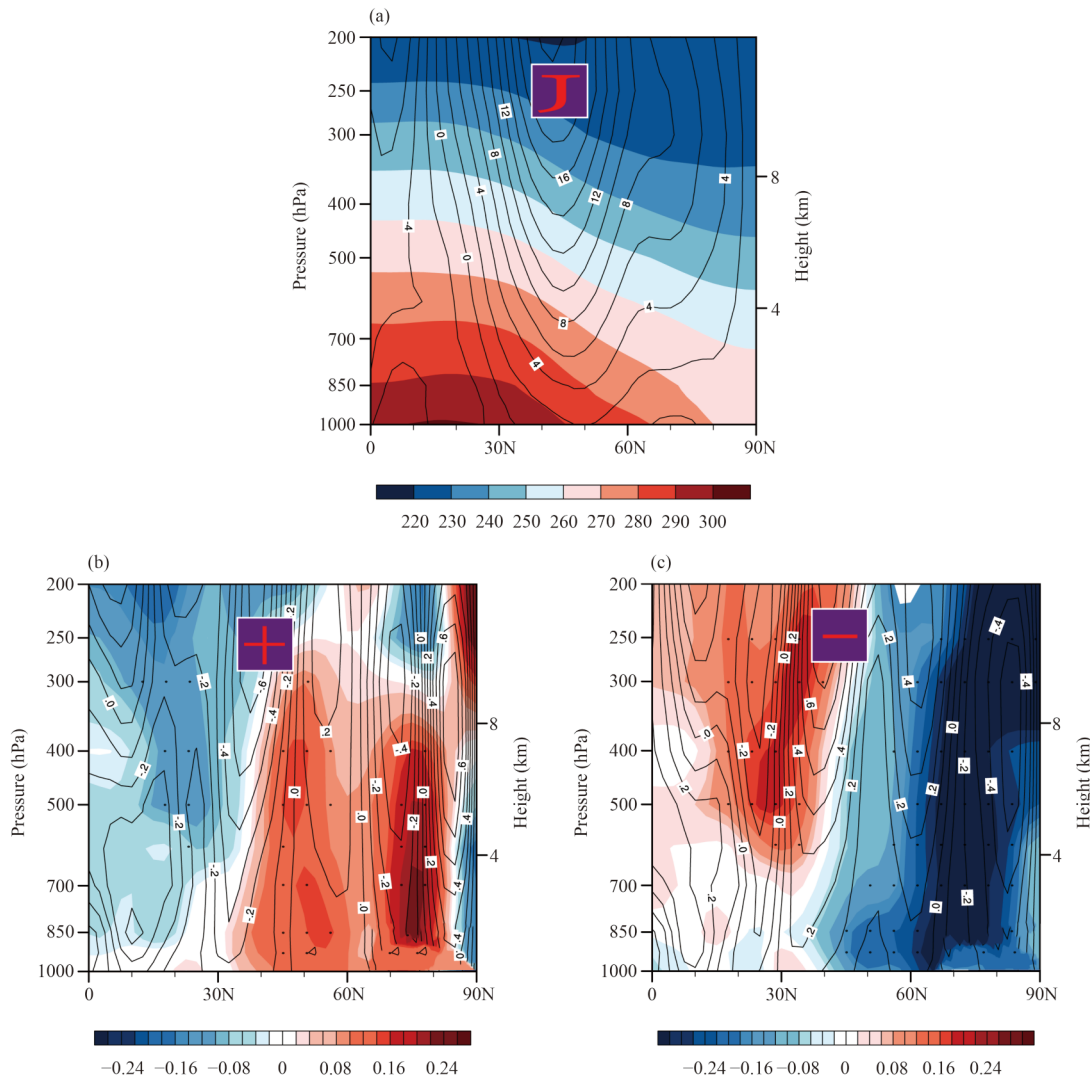
Fig. 8. (a) Vertical–meridional cross-section of zonal mean climatological summer mean temperature (shaded; K) and zonal wind (contour; m s^{-1}) fields averaged during May–October. Vertical–meridional cross-sections of zonal mean intraseasonal temperature (shaded; K) and zonal wind (contour; m s^{-1}) anomalies during (b) Phases 1–2 and (c) Phases 5–6. Black dots represent values exceeding the 95% confidence level (Student *t*-test).

downward motion to the north and anomalous ascending motion to the south. The downward motion further causes a positive temperature anomaly due to adiabatic warming. As a result, a maximum warming center appears in North Pacific north of 40°N. Both the anomalous subsidence and tropospheric warming during Phases 1–2 modulate high-frequency perturbations, favoring more frequent extreme hot events.

The same physical argument can be applied to the low-frequency wind and temperature changes during Phase 5–6. That is, a strengthened jet leads to anomalous ascending motion and thus cold temperature anomalies in North Pacific north of the climatological jet stream. The change of the low-frequency environmental condition further favors the occurrence of extreme cool events in

situ.

In addition to its effect on the jet intensity, the BSISO may directly exert a planetary scale vertical overturning circulation to affect the extreme events in North Pacific and North America. Figure 10 shows the composite velocity potential fields at 200 and 850 hPa. The velocity potential fields reflect large-scale overturning circulation in the troposphere. As one can see, a large-scale upper-level divergence center and a low-level convergence center appear in the tropical Indian Ocean, while an opposite sign happens in the tropical Pacific. The zonally oriented wavenumber-1 pattern is a result of enhanced precipitation anomalies in both the Indian monsoon region and the East Asian monsoon (Meiyu front) region. The former may induce a large-scale east–west circulation, as poin-
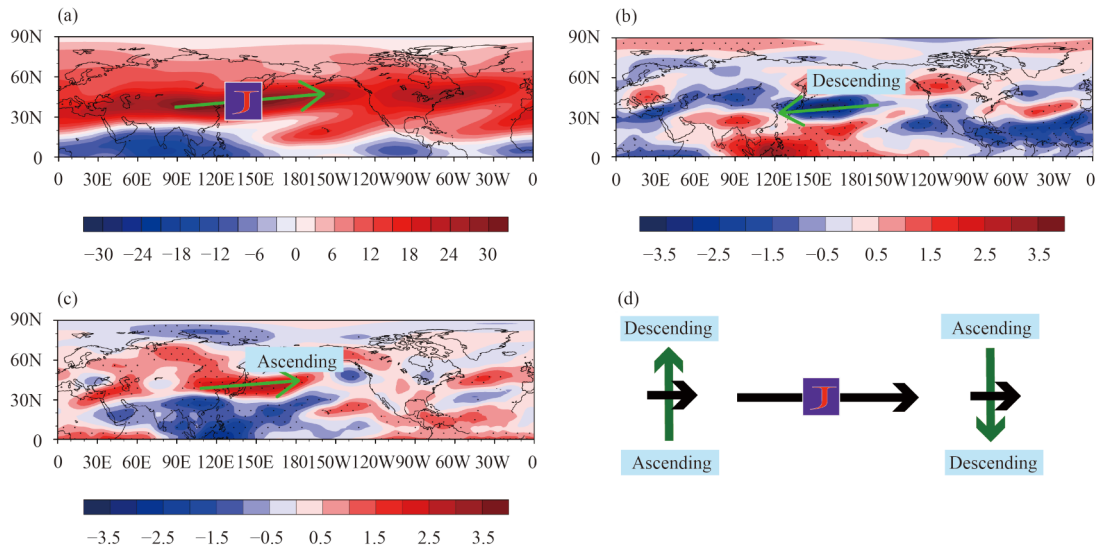
Fig. 9. (a) Horizontal distribution of climatological summer mean zonal wind (m s^{-1}) at 200 hPa averaged during 1983–2012 (green arrow represents the jet center). Horizontal distribution of anomalous zonal wind (m s^{-1}) at 200 hPa during BSISO (b) Phases 1–2 and (c) Phases 5–6. Black dots represent values exceeding the 95% confidence level (Student t-test). (d) Schematic diagram illustrating the upper-level ageostrophic wind vector (green) associated with the summer mean subtropical jet and so induced vertical velocity anomalies in the middle troposphere.
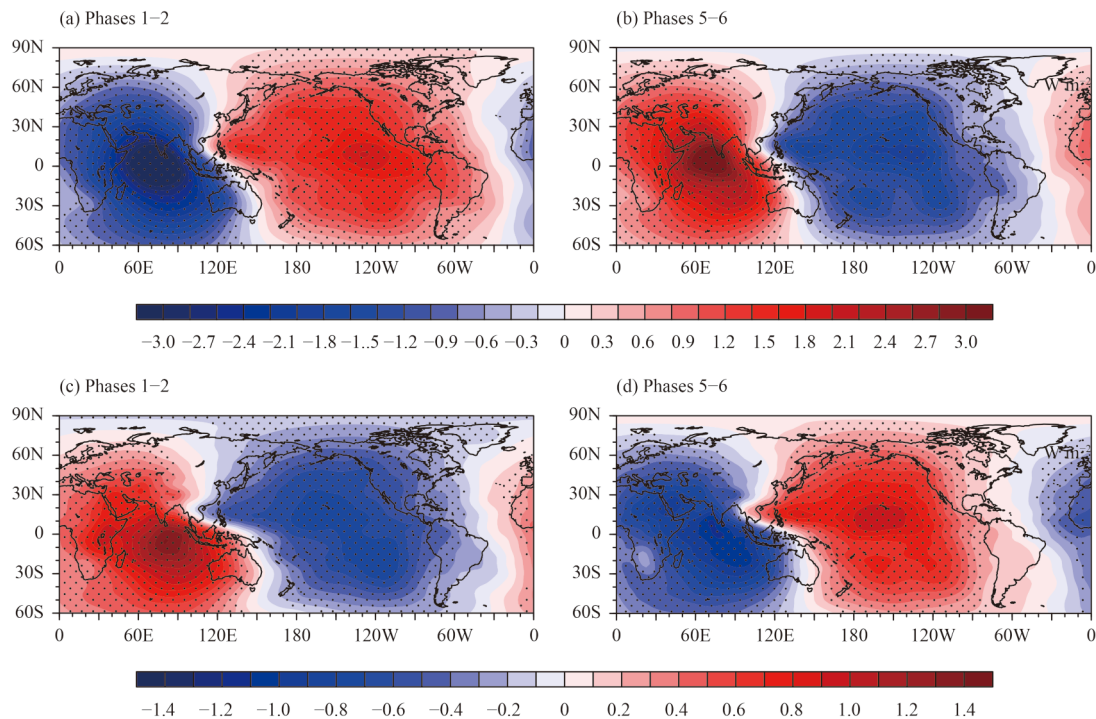

Fig. 10. Composite velocity potential anomaly (s^{-1}) fields at (a, b) 200 and (c, d) 850 hPa with a 3–9-day lag for BSISO1 (a, c) Phases 1–2 and (b, d) Phases 5–6. Black dots represent values exceeding the 95% confidence level (Student t-test).

ted out by Krishnamurti (1971), while the latter is responsible for the formation of a transverse monsoon, as discussed by Webster et al. (1998). The so-induced large-scale subsidence in the Pacific acts together with the aforementioned subtropical jet effect, leading to strong descending motion anomalies and thus warm in-

traseasonal temperature anomalies over North Pacific (Fig. 8b). These intraseasonal anomalies increase the chance of extreme hot events in situ.

The increase of extreme hot events over North America may arise from both the wave train effect and the east–west velocity potential dipole. One can see from

Fig. 6 that there is a high pressure anomaly center over the western coast of United States. This anomalous pressure center increases with height. This leads to a positive temperature anomaly in situ, according to the hydrostatic approximation. As a result, extreme hot events are also observed in North America during Phases 1–2 (Fig. 4a).

5. Role of tropical heating in generating circulation anomalies in midlatitudes: Anomaly GCM experiments

To prove that the observed wave train pattern in North Pacific is indeed a result of the tropical forcing associated with the BSISO, we conducted anomalous atmospheric GCM experiments with a specified heating profile in the tropical Indian Ocean and western Pacific (15°S–30°N, 40°–160°E). The observed summer mean state is specified as the model basic state. The horizontal pattern of the heating anomaly is derived from those shown in Fig. 5a. The heating has an idealized vertical profile with a maximum at the middle troposphere.

Figure 11 shows the simulated upper-level (300 hPa) geopotential height anomaly field averaged during the last 30 days. A wave train pattern is clearly seen, and the wave train pattern resembles the observed during Phases 1–2. Over the forcing region (20°N, 120°E), there is an anomalous low pressure center. Away from the forcing region, a high pressure center appears over northeast of Japan, followed by a low pressure center over Alaska, and a high pressure center over the western coast of United States. Thus, the numerical model result confirms the hypothesis that the wave train pattern is caused by the tropical heating associated with the BSISO.

A further examination of the anomalous geopotential height field in lower levels confirms the equivalent barotropic structure for the wave train in midlatitudes. Similar to the observation, the simulated wind field shows clearly anomalous easterlies over the climatological jet stream, leading to a weakening of the jet and thus a reversed me-

Fig. 11. Simulated geopotential height anomaly (gpm) field at 300 hPa from an anomaly atmospheric GCM in response to anomalous heating in the tropics during BSISO Phases 1–2.

ridional temperature gradient anomaly.

6. Summary

A number of studies have been devoted to understand the role of the BSISO in causing low-frequency precipitation and temperature anomalies as well as extreme temperature events over the Asian monsoon region (e.g., Webster et al., 1998; Annamalai and Slingo, 2001; Mao and Wu, 2006; Yang et al., 2010; Chen et al., 2015; Hsu et al., 2016, 2017). However, less studies have been done in understand the remote impact of the BSISO on extreme temperatures events in middle- and high-latitude Northern Hemisphere. In this study, we analyzed the observed relationship between the extreme hot and cool events in the Northern Hemisphere and the BSISO phase, and investigated the mechanism that causes the relationship.

The BSISO phase was defined, following Lee et al. (2013). The extreme hot or cool events are defined when daily mean temperature exceeds the 95th percentile or lower than the 5th percentile. Our analysis result shows that there are more frequent extreme hot (cool) events in the Northern Hemisphere, in particular over North Pacific, North America, and polar region north of 60°N, 3–9 days after BSISO Phases 1–2 (Phases 5–6). The probability for occurrence of extreme hot events in these regions is 40% more than that for occurrence of non-extreme hot events during Phases 1–2. A similar result is found for occurrence of extreme cool events during Phases 5–6.

Two physical processes are responsible for the increased frequency of extreme hot events over North Pacific. The first is the Rossby wave train (Hoskins and Karoly, 1981) triggered by a negative heating anomaly in the WNP associated with the BSISO Phases 1–2. In response to the negative heating, a low-pressure anomaly and a convergence anomaly appear over the upper troposphere in situ. The upper-level convergence anomaly acts as a Rossby wave vorticity source, triggering a Rossby wave train into higher latitudes, and forming a big circle with alternated high–low–high pressure anomaly centers (Hoskins and Karoly, 1981). Within the Rossby wave train, two strong high pressure anomaly centers stand out along 40°N, with one center over the northeast of Japan and the other center over western coast of United States. The anomalous high pressure systems, on one hand, are accompanied by tropospheric warm temperature anomalies according to the hydrostatic relationship, and on the other hand, induce anomalous easterlies to the south, weakening the climatological subtropical jet. The weak-
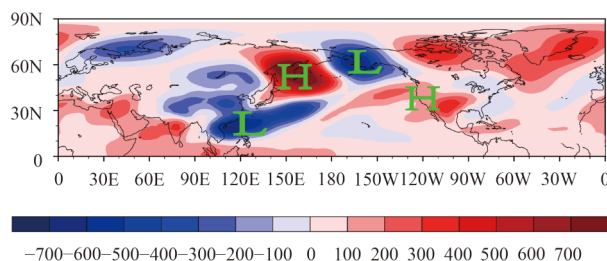
ening of the jet causes anomalous subsidence to the northeast of the subtropical jet, favoring extreme hot events there. The second process is through the transverse monsoon (Webster et al., 1998) and large-scale east–west circulation (Krishnamurti, 1971)—the heating anomalies over South Asia and East Asia generate a zonal wavenumber-1 velocity potential dipole, with anomalous ascending motion over tropical Indian Ocean and large-scale anomalous subsidence over the Pacific and North America. Both the processes induce abnormal descending motion and temperature warming over midlatitude North Pacific and higher-latitude polar regions, favoring the occurrence of extreme hot events there.

An anomaly atmospheric GCM is used to test whether a specified tropical heating anomaly associated with the BSISO can indeed induce the observed Rossby wave train pattern in midlatitudes. The numerical model result confirms our hypothesis, that is, the precipitation anomaly in the tropics associated with the BSISO can alter upper-level divergent flow and induce a Rossby wave train with prominent pressure anomalies over northeast of Japan and the western coast of United States. The associated wind change can further modify the subtropical jet stream and result in the observed temperature anomalies over the Northern Hemisphere.

The BSISO–extreme event relationship revealed by the current study may be applied to operational extended-range (10–30 days) weather forecast. Either a pure statistical model such as that done by Zhu and Li (2017) or a combined dynamical–statistical model may be constructed based on the above relationship. In the latter case, selecting a dynamical model that has a good forecast skill of the BSISO is critical. We plan to conduct such extended-range forecast experiments in near future.

REFERENCES

Annamalai, H., and J. M. Slingo, 2001: Active/break cycles: Diagnosis of the intraseasonal variability of the Asian summer monsoon. *Climate Dyn.*, **18**, 85–102, doi: 10.1007/s0038 20100161.

Chen, J. P., Z. P. Wen, R. G. Wu, et al., 2015: Influences of northward propagating 25–90-day and quasi-biweekly oscillations on eastern China summer rainfall. *Climate Dyn.*, **45**, 105–124, doi: 10.1007/s00382-014-2334-y.

Chen, R. D., Z. P. Wen, and R. Y. Lu, 2018: Large-scale circulation anomalies and intraseasonal oscillations associated with long-lived extreme heat events in South China. *J. Climate*, **31**, 213–232, doi: 10.1175/JCLI-D-17-0232.1.

Chen, Y., and P. M. Zhai, 2017: Simultaneous modulations of precipitation and temperature extremes in southern parts of China by the boreal summer intraseasonal oscillation. *Climate Dyn.*, **49**, 3363–3381, doi: 10.1007/s00382-016-3518-4.

Ebisuzaki, W., 1997: A method to estimate the statistical significance of a correlation when the data are serially correlated. *J. Climate*, **10**, 2147–2153, doi: 10.1175/1520-0442(1997)010 <2147:AMTETS>2.0.CO;2.

Held, I. M., and M. J. Suarez, 1994: A proposal for the intercomparison of the dynamical cores of atmospheric general circulation models. *Bull. Amer. Meteor. Soc.*, **75**, 1825–1830, doi: 10.1175/1520-0477(1994)075<1825:APFTIO>2.0.CO;2.

Hendon, H. H., and M. L. Salby, 1994: The life cycle of the Madden–Julian Oscillation. *J. Atmos. Sci.*, **51**, 2225–2237, doi: 10.1175/1520-0469(1994)051<2225:TLCOTM>2.0.CO;2.

Hoskins, B. J., and D. J. Karoly, 1981: The steady linear response of a spherical atmosphere to thermal and orographic forcing. *J. Atmos. Sci.*, **38**, 1179–1196, doi: 10.1175/1520-0469(1981) 038<1179:TSLROA>2.0.CO;2.

Hsu, P. C., J. Y. Lee, and K. J. Ha, 2016: Influence of boreal summer intraseasonal oscillation on rainfall extremes in southern China. *Int. J. Climatol.*, **36**, 1403–1412, doi: 10.1002/joc. 4433.

Hsu, P. C., J. Y. Lee, K. J. Ha, et al., 2017: Influences of boreal summer intraseasonal oscillation on heat waves in Monsoon Asia. *J. Climate*, **30**, 7191–7211, doi: 10.1175/JCLI-D-16-0505.1.

Jiang, X. A., T. Li, and B. Wang, 2004: Structures and mechanisms of the northward propagating boreal summer intraseasonal oscillation. *J. Climate*, **17**, 1022–1039, doi: 10.1175/1520-0442(2004)017<1022:SAMOTN>2.0.CO;2.

Jiang, X. A., and T. Li, 2005: Reinitiation of the boreal summer intraseasonal oscillation in the tropical Indian Ocean. *J. Climate*, **18**, 3777–3795, doi: 10.1175/JCLI3516.1.

Kemball-Cook, S., and B. Wang, 2001: Equatorial waves and air–sea interaction in the boreal summer intraseasonal oscillation. *J. Climate*, **14**, 2923–2942, doi: 10.1175/1520-0442 (2001)014<2923:EWAASI>2.0.CO;2.

Krishnamurti, T. N., 1971: Tropical east–west circulations during the northern summer. *J. Atmos. Sci.*, **28**, 1342–1347, doi: 10.1175/1520-0469(1971)028<1342:TEWCDT>2.0.CO;2.

Lau, K. M., and P. H. Chan, 1986: Aspects of the 40–50-day oscillation during the northern summer as inferred from outgoing longwave radiation. *Mon. Wea. Rev.*, **114**, 1354–1367, doi: 10.1175/1520-0493(1986)114<1354:AOTDOD>2.0.CO;2.

Lee, J. Y., B. Wang, M. C. Wheeler, et al., 2013: Real-time multivariate indices for the boreal summer intraseasonal oscillation over the Asian summer monsoon region. *Climate Dyn.*, **40**, 493–509, doi: 10.1007/s00382-012-1544-4.

Li, C. Y., 2000: Introduction of Climate Dynamics. 2nd ed., China Meteorological Press, Beijing, 449 pp. (in Chinese)

Li, T., 2006: Origin of the summertime synoptic-scale wave train in the western North Pacific. *J. Atmos. Sci.*, **63**, 1093–1102, doi: 10.1175/JAS3676.1.

Li, T., 2010: Monsoon climate variabilities. *Climate Dynamics: Why Does Climate Vary?* D. Z. Sun and B. Frank, Eds., American Geophysical Union, Washington, D.C., doi: 10.1029/2008GM000782

Li, T., and B. Wang, 2005: A review on the western North Pacific monsoon: Synoptic-to-interannual variabilities. *Terrestrial, Atmospheric and Oceanic Sciences*, **16**, 285–314, doi: 10.33 19/TAO.2005.16.2.285(A).

Li, T., and P. C. Hsu, 2017: *Fundamentals of Tropical Climate Dy-*

namics. Springer, Cham, doi: 10.1007/978-3-319-59597-9.

Li, T. M., 2014: Recent advance in understanding the dynamics of the Madden–Julian oscillation. *J. Meteor. Res.*, **28**, 1–33, doi: 10.1007/s13351-014-3087-6.

Liebmann, B., and C. A. Smith, 1996: Description of a complete (interpolated) outgoing longwave radiation dataset. *Bull. Amer. Meteor. Soc.*, **77**, 1275–1277.

Madden, R. A., and P. R. Julian, 1971: Detection of a 40–50 day oscillation in the zonal wind in the tropical Pacific. *J. Atmos. Sci.*, **28**, 702–708, doi: 10.1175/1520-0469(1971)028<0702: DOADOI>2.0.CO;2.

Madden, R. A., and P. R. Julian, 1972: Description of global-scale circulation cells in the tropics with a 40–50 day period. *J. Atmos. Sci.*, **29**, 1109–1123, doi: 10.1175/1520-0469(1972)029 <1109:DOGSCC>2.0.CO;2.

Mao, J. Y., and G. X. Wu, 2006: Intraseasonal variations of the Yangtze rainfall and its related atmospheric circulation features during the 1991 summer. *Climate Dyn.*, **27**, 815–830, doi: 10.1007/s00382-006-0164-2.

Matsueda, S., and Y. Takaya, 2015: The global influence of the Madden–Julian oscillation on extreme temperature events. *J. Climate*, **28**, 4141–4151, doi: 10.1175/JCLI-D-14-00625.1.

Murakami, T., 1980: Empirical orthogonal function analysis of satellite-observed outgoing longwave radiation during summer. *Mon. Wea. Rev.*, **108**, 205–222, doi: 10.1175/1520-0493(1980)108<0205:EOFAOS>2.0.CO;2.

Ren, B. H., and R. H. Huang, 2002: 10–25-day intraseasonal variations of convection and circulation associated with thermal state of the western Pacific warm pool during boreal summer. *Adv. Atmos. Sci.*, **19**, 321–336, doi: 10.1007/s00376-002-0025-9.

Sun, G. W., F. Xin, B. M. Chen, et al., 2008: A predicting method on the low-frequency synoptic weather map. *Plateau Meteor.*, **27**, 64–68. (in Chinese)

Wang, B., R. G. Wu, and T. Li, 2003: Atmosphere–warm Ocean interaction and its impacts on Asian–Australian Monsoon variation. *J. Climate*, **16**, 1195–1211, doi: 10.1175/1520-0442(2003)16<1195:AOIAII>2.0.CO;2.

Webster, P. J., V. O. Magaña, T. N. Palmer, et al., 1998: Monsoons: Processes, predictability, and the prospects for prediction. *J. Geophys. Res.*, **103**, 14451–14510, doi: 10.1029/97JC02719.

Weickmann, K. M., 1983: Intraseasonal circulation and outgoing longwave radiation modes during Northern Hemisphere winter. *Mon. Wea. Rev.*, **111**, 1838–1858, doi: 10.1175/1520-0493(1983)111<1838:ICAOLR>2.0.CO;2.

Wheeler, M. C., and H. H. Hendon, 2004: An all-season real-time multivariate MJO index: Development of an index for monitoring and prediction. *Mon. Wea. Rev.*, **132**, 1917–1932, doi: 10.1175/1520-0493(2004)132<1917:AARMMI>2.0.CO;2.

Wu, B., T. J. Zhou, and T. Li, 2016: Impacts of the Pacific–Japan and circumglobal teleconnection patterns on the interdecadal variability of the East Asian summer monsoon. *J. Climate*, **29**, 3253–3271, doi: 10.1175/JCLI-D-15-0105.1.

Yang, J., B. Wang, Q. Bao, et al., 2010: Biweekly and 21–30-day variations of the subtropical summer monsoon rainfall over the lower reach of the Yangtze River basin. *J. Climate*, **23**, 1146–1160, doi: 10.1175/2009JCLI3005.1.

Yasunari, T., 1979: Cloudiness fluctuations associated with the Northern Hemisphere summer monsoon. *J. Meteor. Soc. Japan*, **57**, 227–242, doi: 10.2151/jmsj1965.57.3_227.

Zhu, Z. W., and T. Li, 2016: A new paradigm for continental U.S. summer rainfall variability: Asia–North America teleconnection. *J. Climate*, **29**, 7313–7327, doi: 10.1175/JCLI-D-16-0137.1.

Zhu, Z. W., and T. Li, 2017: The statistical extended-range (10–30-day) forecast of summer rainfall anomalies over the entire China. *Climate Dyn.*, **48**, 209–224, doi: 10.1007/s003 82-016-3070-2.

Zhu, Z. W., T. Li, P. C. Hsu, et al., 2015: A spatial–temporal projection model for extended-range forecast in the tropics. *Climate Dyn.*, **45**, 1085–1098, doi: 10.1007/s00382-014-2353-8.

Tech & Copy Editor: Hongqun ZHANG